

RESEARCH ARTICLE

Accelerated magnetic resonance fingerprinting using soft-weighted key-hole (MRF-SOHO)

Gastao Cruz^{1*}, Torben Schneider², Tom Bruijnen³, Andreia S. Gaspar⁴, René M. Botnar^{1,5}, Claudia Prieto^{1,5}

1 School of Biomedical Engineering and Imaging Sciences, King's College London, London, United Kingdom, **2** Philips Healthcare, Guilford, United Kingdom, **3** Department of Radiotherapy, University Medical Center Utrecht, Utrecht, The Netherlands, **4** Institute for Systems and Robotics / Department of Bioengineering, Instituto Superior Técnico, Universidade de Lisboa, Lisbon, Portugal, **5** Escuela de Ingeniería, Pontificia Universidad Católica de Chile, Santiago, Chile

* gastao.cruz@kcl.ac.uk



Abstract

OPEN ACCESS

Citation: Cruz G, Schneider T, Bruijnen T, Gaspar AS, Botnar RM, Prieto C (2018) Accelerated magnetic resonance fingerprinting using soft-weighted key-hole (MRF-SOHO). PLoS ONE 13(8): e0201808. <https://doi.org/10.1371/journal.pone.0201808>

Editor: Jan Fritz, Johns Hopkins School of Medicine, UNITED STATES

Received: January 3, 2018

Accepted: July 23, 2018

Published: August 9, 2018

Copyright: © 2018 Cruz et al. This is an open access article distributed under the terms of the [Creative Commons Attribution License](https://creativecommons.org/licenses/by/4.0/), which permits unrestricted use, distribution, and reproduction in any medium, provided the original author and source are credited.

Data Availability Statement: Data has been uploaded to figshare.com with the following DOI: [10.6084/m9.figshare.6866075](https://doi.org/10.6084/m9.figshare.6866075).

Funding: The authors acknowledge financial support from the following: EPSRC: EPSRC EP/P001009/. URL: <http://gow.epsrc.ac.uk/NGBOViewGrant.aspx?GrantRef=EP/P001009/1>. FONDECYT: 1161055. URL: <http://www.conicyt.cl/fondecyt/files/2015/04/No%CC%81mina-de-proyectos-aprobados-Regular-2016.pdf>. The Centre of Excellence in Medical Engineering funded

Object

To develop a novel approach for highly accelerated Magnetic Resonance Fingerprinting (MRF) acquisition.

Materials and methods

The proposed method combines parallel imaging, soft-gating and key-hole approaches to highly accelerate MRF acquisition. Slowly varying flip angles (FA), commonly used during MRF acquisition, lead to a smooth change in the signal contrast of consecutive time-point images. This assumption enables sharing of high frequency data between different time-points, similar to what is done in some dynamic MR imaging methods such as key-hole. The proposed approach exploits this information using a SOft-weighted key-HOle (MRF-SOHO) reconstruction to achieve high acceleration factors and/or increased resolution without compromising image quality or increasing scan time. MRF-SOHO was validated on a standard T₁/T₂ phantom and in *in-vivo* brain acquisitions reconstructing T₁, T₂ and proton density parametric maps.

Results

Accelerated MRF-SOHO using less data per time-point and less time-point images enabled a considerable reduction in scan time (up to 4.6x), while obtaining similar T₁ and T₂ accuracy and precision when compared to zero-filled MRF reconstruction. For the same number of spokes and time-points, the proposed method yielded an enhanced performance in quantifying parameters than the zero-filled MRF reconstruction, which was verified with 2, 1 and 0.7 (sub-millimetre) resolutions.

by the Wellcome Trust (WT 088641/Z/09/Z). URL: <https://wellcome.ac.uk/funding/managing-grant/grants-awarded>. The Department of Health via the National Institute for Health Research (NIHR) comprehensive Biomedical Research Centre award to Guy's & St Thomas' NHS Foundation Trust in partnership with King's College London and King's College Hospital NHS Foundation Trust. URL: <https://www.nihr.ac.uk/>. All funders had a role in study design, data collection, analysis and preparation of manuscript. The views expressed are those of the authors and not necessarily those of the NHS, the NIHR or the Department of Health.

Competing interests: One of the co-authors (Torben Schneider) is an employee of Philips Healthcare. Following the regulation on Competing Interests Statement, I confirm that this does not alter our adherence to PLOS ONE policies on sharing data and materials.

Conclusion

The proposed MRF-SOHO enabled a 4.6x scan time reduction for an in-plane spatial resolution of $2 \times 2 \text{ mm}^2$ when compared to zero-filled MRF and enabled sub-millimetric ($0.7 \times 0.7 \text{ mm}^2$) resolution MRF.

Introduction

Quantitative Magnetic Resonance Imaging (MRI) techniques, such as T_1 , T_2 and proton density (M_0) parametric maps, have been developed to enable direct objective comparison and characterization of diseased and healthy tissue [1–6]. However, current quantitative MRI methods are slow and typically provide single parameter information per acquisition. Therefore different parameters need to be measured in serial acquisitions, further increasing the scan time. Magnetic Resonance Fingerprinting (MRF) [7] has been recently introduced to retrieve multiple and simultaneous parametric maps from a single acquisition under the assumption that unique signal evolutions or “fingerprints” can be generated from different tissues. This is achieved using a variable encoding and acquisition scheme that typically varies flip angles (FA) and repetition times (TR) throughout the scan. Since there are little constraints regarding the acquired signal, MRF is exceptionally flexible in terms of pulse sequence design. Multiple parameters are reconstructed in MRF via pixel-wise template matching of a measured signal (series of time-point images) to a previously generated dictionary of signals. Generally, template matching is achieved by finding the dictionary entry with the highest inner product with the fingerprint in a given pixel, via exhaustive search. The dictionary needs to contain signal evolutions from all potential tissues of interest subject to a set of sequence parameters, thus all MR parameters employed to generate the dictionary of fingerprints can be reconstructed simultaneously. Dictionaries have been generated using Bloch equation or extended phase graph formalisms to simulate the acquisition sequence [8]. MRF reconstruction has been shown to be robust to measurement noise and incoherent undersampling artefacts, provided a large number (~ 1000) of time-point images are acquired, and therefore highly undersampled time-point images have been employed [7]. In spite of the high undersampling factors reported, the large amount of time point images required in MRF may result in long acquisitions for some important applications such as high-resolution 2D breath hold acquisitions and high-resolution 3D scans. Moreover the low quality of the highly undersampled time-point images can introduce bias in the parametric values if the template matching based MRF reconstruction fails to distinguish between signal and noise or undersampling artefacts [9].

Recent work has focused on investigating the feasibility of MRF for different applications, as well as improving the MRF framework itself. MRF has been combined with simultaneous multi-slice acquisition [10] at an acceleration factor of two and with echo-planar imaging [11] to simultaneously measure T_1 and T_2^* . B_1 estimation has been incorporated into the signal simulation in 2D and 3D MRF, enabling measurements of T_1 , T_2 and B_1 with increased accuracy [12, 13]. Myocardial MRF in 2D using magnetization preparation pulses and cardiac triggering has been developed, showing good agreement with gold standard methods [14]. Template matching durations have also been significantly reduced using fast group matching algorithms [15]. In [16], a multi-scale MRF reconstruction was introduced, improving measurement accuracy and significantly reducing the number of time-point images required. More recently a sliding window reconstruction was proposed to improve T_1 and T_2 measurement accuracy and/or reduce acquisition time [17]. The low rank nature of the dictionary has

been leveraged to improve parametric map quality and reduce the number of Fourier transforms required [18]. A maximum likelihood formulation has been introduced [19], also accelerating the number of time-points. With the high acceleration factors typically employed in MRF ($R > 20$), the parallel imaging reconstruction is very ill-posed. With sufficient a priori information the linear problem can be solved, producing high quality time-point images and consequently improving the parametric maps.

In this work, we develop a novel reconstruction approach for highly accelerated MRF acquisition. The proposed SOft-weighted key-HOle (MRF-SOHO) reconstruction enables shorter acquisition times (higher acceleration factor per time-point image and/or reduced number of time-points), and improved sub-millimetre in-plane resolution. This is achieved by considerably improving the quality of the time-point images with a reconstruction based on parallel imaging [20], soft-gating [21] and key-hole [22] methods. Slow FA variation between time-point images is commonly used in MRF to explore the parametric space, generating unique fingerprints. This continuous change in magnetization leads to a smooth change in contrast through the time-point images, resulting in redundant high spatial frequency information. MRF-SOHO exploits this redundancy by using a soft-weighted iterative SENSE reconstruction to share high-frequency data between consecutive time-point images. The proposed approach was validated on a standardized T_1/T_2 phantom and in *in-vivo* brain data in three healthy subjects.

Materials and methods

Data acquisition

Gradient echo readout with variable FA and TR after an initial inversion pulse was used for data acquisition as proposed in [23]. A golden radial trajectory [24] was employed instead of the spiral trajectory used in [23]. However, multiple radial spokes may be required per time-point image. To this end, the acquisition scheme in [23] was modified such that the FA and TR corresponding to time point t (FA_t and TR_t , respectively) were repeated N_p times, where N_p is the number of radial spokes per time-point image. The FA was given by:

$$FA_t = \sin\left(\frac{[t/N_p + 1]\pi}{N_{rf}}\right) FA_{max}$$

where N_{rf} is the number of RF pulses per section of the acquisition and FA_{max} is the maximum FA in the corresponding section. The TR pattern followed a pseudo random Perlin noise. Both FA and TR patterns are further described in [23].

Reconstruction of time-point images

The proposed MRF-SOHO reconstruction relies on high-frequency data redundancy of neighbouring time-point images under the assumption of smoothly varying contrast. Information is shared between neighbouring time-point images I_t using an iterative SENSE soft-weighted reconstruction given by:

$$\hat{I}_t = \arg \min_t \{ \|W_t^n(FSI_t - K)\|_2^2 \}$$

where F is the Fourier transform (including non-Cartesian density compensation and non-uniform Fourier transform), S are the coil sensitivities and K are the acquired k-space data for all time-points. Equation 2 was solved with the Conjugate Gradient method. The soft-weights

W_t^n for time-point t and neighbor $n \in \{t - \Delta t, t - \Delta t + 1, \dots, t + \Delta t - 1, t + \Delta t\}$ are given by:

$$W_t^n(k_r) = G_t^n \cdot \left\{ 1 - \left[\exp\left(\frac{k_r - \alpha(n)}{\beta(n)}\right) + 1 \right]^{-1} \right\}, \quad \text{if } n \neq t$$

$$W_t^n(k_r) = 1, \quad \text{if } n = t$$

$$G_t^n = \left[\exp\left(\frac{|FA_t - FA_n| - \mu}{\tau}\right) + 1 \right]^{-1}$$

where k_r is the k-space distance from the corresponding sample to the k-space centre, α is the distance at which $W_t^n(\alpha) = 0.5$ and β determines the smoothness of the transition from $W_t^n(k_r) \cong 0$ to $W_t^n(k_r) \cong 1$. G_t^n determines how much data is shared as a function of the relative change in the FA: the faster the rate of change in FA, the faster the change in contrast and therefore the less the data that can be shared. μ determines the threshold where data sharing is reduced and τ determines the smoothness of that transition. Through parameters α, β, μ, τ and Δt this distribution can be adjusted to adequately share data between neighbouring time-points without compromising image contrast. A pictorial diagram of the data shared can be seen in Fig 1 with one radial spoke per excitation and a neighbourhood size ($N = 2\Delta t + 1$) of 5. Some high spatial frequency data is always shared within the neighbourhood, however the amount of low frequency data shared depends on the distance between time-point neighbours. Soft-weights, FAs and corresponding time-point images are shown in Fig 2. Representative time-point reconstructions with gridding, as in zero-filled MRF, and with MRF-SOHO demonstrate an improvement in time-points image quality while maintaining contrast. An example plot of soft-weights for $N = 11$ is shown in Fig 2, indicating the fraction of data shared as a function of the k-space distance to the centre. A plot of the flip angle pattern used and an example plot of the soft-weighting functions are also shown in Fig 2.

Dictionary and pattern recognition

The MRF dictionaries were simulated using the Extended Phase Graph (EPG) formalism [8, 25], based on code available in [25] for different T_1 and T_2 values. B_1 and RF slice profile were not incorporated into the dictionary. T_1, T_2 and M_0 parametric maps were obtained via

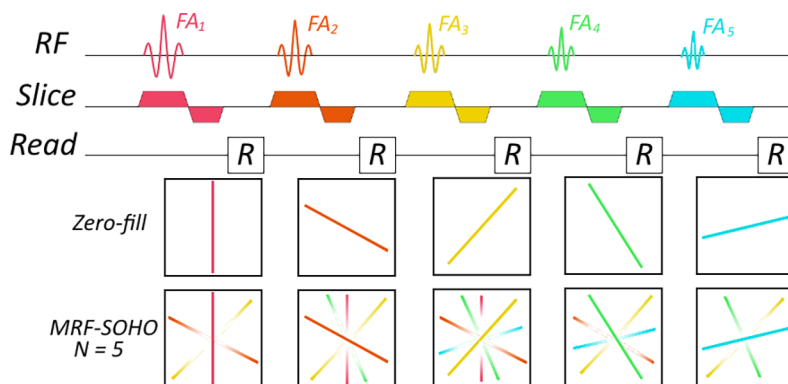


Fig 1. Pictorial diagram of MRF-SOHO's data sharing scheme. The example depicted features a neighbourhood size (N) of 5, with one radial profile per flip angle (N_p). The transparency of colour indicates the fraction of data shared. The farther away the time-point, the less low frequency data is shared.

<https://doi.org/10.1371/journal.pone.0201808.g001>

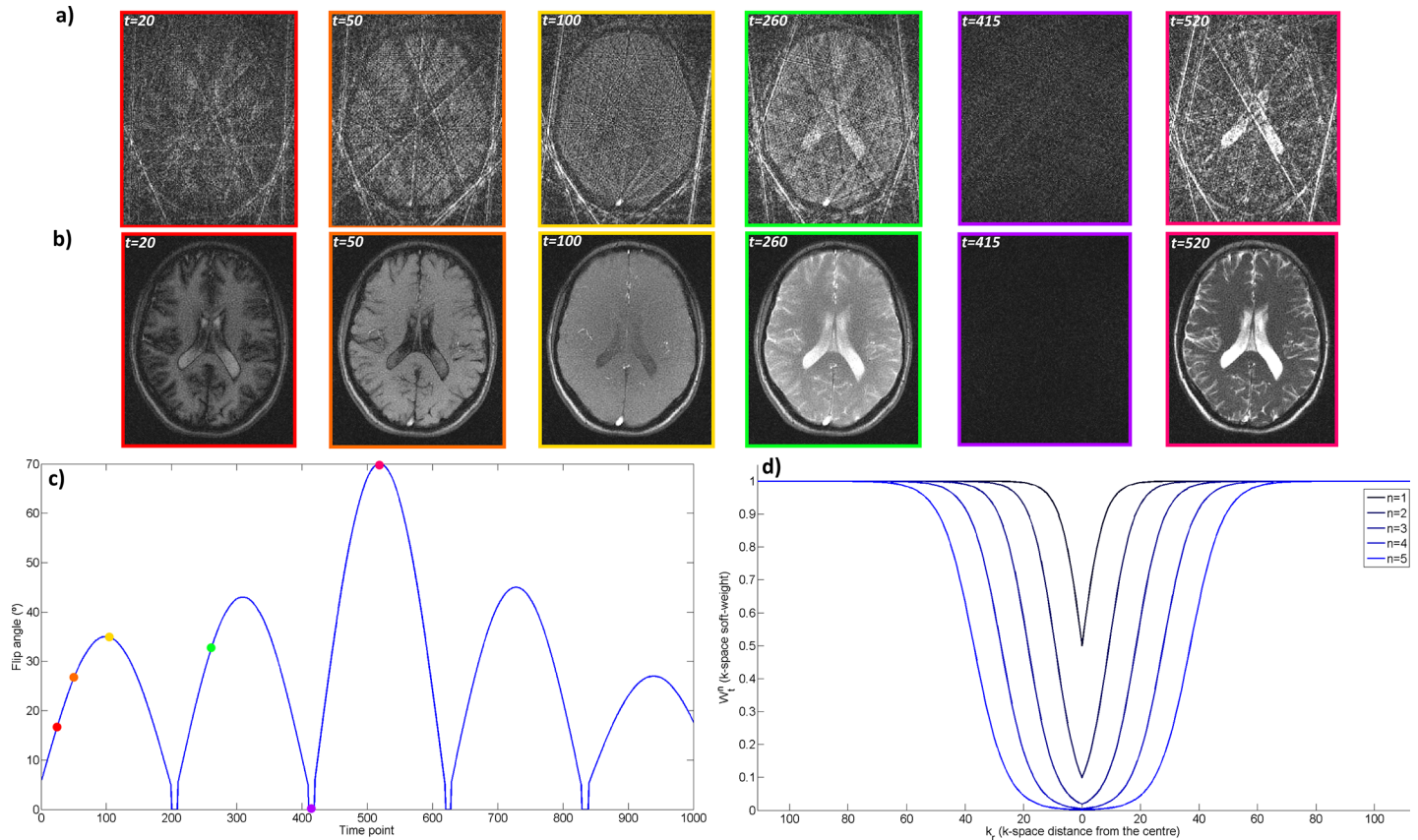


Fig 2. Time-points, flip angle pattern and soft-weights. **a)** Gridding reconstruction used in zero-filled MRF at different time-points in the acquisition, with 8 spokes per time-point. **b)** MRF-SOHO reconstruction at different time-points in the acquisition. High quality images are reconstructed at each time point with MRF-SOHO without affecting image contrast. **c)** Flip angle pattern used presents a smooth evolution. Coloured time-points correspond to the images above. **d)** Soft-weights (W_i^n) for different neighbouring time-points (n) as a function of k-space radial distance (k_r). The further away the time point, the less low frequency data is shared.

<https://doi.org/10.1371/journal.pone.0201808.g002>

template matching as in [23]. The inner product between the temporal signal from each pixel and all dictionary entries was performed. The highest inner product indicated the correct dictionary entry for each pixel. M_0 parametric maps were calculated as the ratio between the signal and the normalized dictionary entry for each pixel.

Experiments

Data acquisition

Phantom and *in-vivo* brain data was acquired on a 1.5T Ingenia MR system (Philips, Best, The Netherlands) using a 12-element head coil. The study was approved by the institutional review board (London Bridge Research Ethics Committee) and written informed consent was obtained from all subjects according to institutional guidelines.

2D acquisitions were performed on a standardized T_1/T_2 phantom [26] and in three healthy subjects. For both phantom and *in-vivo* acquisitions data was acquired with a gradient echo readout after an initial inversion pulse using a golden radial trajectory. In each case acquisitions were performed with three different in-plane resolutions of 1) $2 \times 2 \text{ mm}^2$, 2) $1 \times 1 \text{ mm}^2$ and 3) $0.7 \times 0.7 \text{ mm}^2$. The respective TRs varied between 1) 3.2 and 4.0 ms, 2) 4.7 and 5.7 ms, and 3) 5.8 and 7.2 ms. The respective TEs were: 1) 1.31 ms, 2) 1.85 ms and 3) 3.2 ms. The remaining relevant parameters were the same for all three acquisitions: 10 mm slice thickness, 260×260

mm² field-of-view, 8 radial spokes per time-point, 1000 time points, one slice. The FA pattern was divided into sections of 200 time-points, with corresponding FA_{max} of 35, 43, 70, 45 and 27 degrees.

Reconstruction of time-point images

Data from the phantom and one subject were reconstructed with different neighbourhood sizes (N), $\alpha(n)$, $\beta(n)$, μ and τ parameters in order to experimentally tune these values. The reconstructions were visually inspected to select the appropriate parameters. Consequently, the MRF-SOHO reconstruction neighbourhood size ($N = 2\Delta t + 1$) was set to 31, $\alpha(n)$ varied linearly between 0 and 20% K_{max} , $\beta(n)$ varied linearly between 1% K_{max} and 2% K_{max} , where K_{max} is the index of the maximum k-space radial point. μ and τ were set to 0.2 and 0.05, respectively. Density compensation function for each time point was obtained via Voronoi diagrams [27] and non-uniform fast Fourier transform based on [28] was employed. The reconstruction was terminated when the relative residual reached 0.05% or when 15 iterations were reached (whichever came first). Coil maps were obtained from all the acquired data using ESPIRiT [29]. The acquired datasets were also reconstructed with a zero-filled gridding reconstruction as in [23]. Both MRF-SOHO and zero-filled MRF reconstructions were performed using 8, 5 and 2 radial profiles per time-point (retrospectively undersampled), corresponding to highly undersampled data. For instance, the 2x2 mm² datasets with 8, 5 and 2 radial profiles per time-point have angular undersampling factors of ~26x, ~41x and ~102x (with respect to a fully sampled radial acquisition) respectively, whereas the 0.7x0.7 mm² datasets with 8, 5 and 2 radial profiles per time-point have angular undersampling factors of ~73x, ~117x and ~292x (with respect to a fully sampled radial acquisition) respectively. Reconstructions were performed off-line in MATLAB (Mathworks, Natick, Massachusetts, USA). MRF-SOHO reconstruction took approximately 10, 30 and 120 minutes to complete for the 2x2, 1x1 and 0.7x0.7 mm² resolution datasets using 8 radial profiles and 1000 time points, respectively. These reconstructions ran on a Linux workstation with 12 Intel Xeon X5675 (3.07 GHz) and 200 GB RAM.

Dictionary and pattern recognition

Dictionaries were tailored for the T₁/T₂ phantom and the brain datasets based on the corresponding tissues. For the phantom and brain data, T₁ ∈ [0:10:400 ms, 400:5:800 ms, 800:20:1400 ms, 1400:200:6000 ms], T₂ ∈ [0:1:150 ms, 150:10:500 ms, 500:50:1000 ms, 1000:200:2600 ms], corresponding to 35496 dictionary entries. For both simulations, B₁ was fixed to 1.0. Template matching of the reconstructed datasets was performed using a different number of time-point images ranging from 50 to 1000 images (with a step size of 50) for both MRF-SOHO and zero-filled MRF.

Results

A considerable improvement in image quality of the time-point images was observed with MRF-SOHO when compared to the zero-filled gridding reconstruction (zero-filled MRF), which is strongly dominated by undersampling artefacts. This can be seen in [S1](#), [S2](#) and [S3](#) Videos, showing the first 500 time-point images reconstructed with zero-filled MRF and MRF-SOHO (using 8 spokes per time-point) in 2 mm², 1 mm² and 0.7 mm², respectively, for subject 1. Inspecting the time-points corresponding to the lowest FA confirms that image contrast is generally unaffected with the proposed approach. Additionally, a variation in image quality can be observed depending on the amount of data shared: regions where contrast changes rapidly (e.g. when the flip angle goes to zero) share less data and therefore have increased residual aliasing.

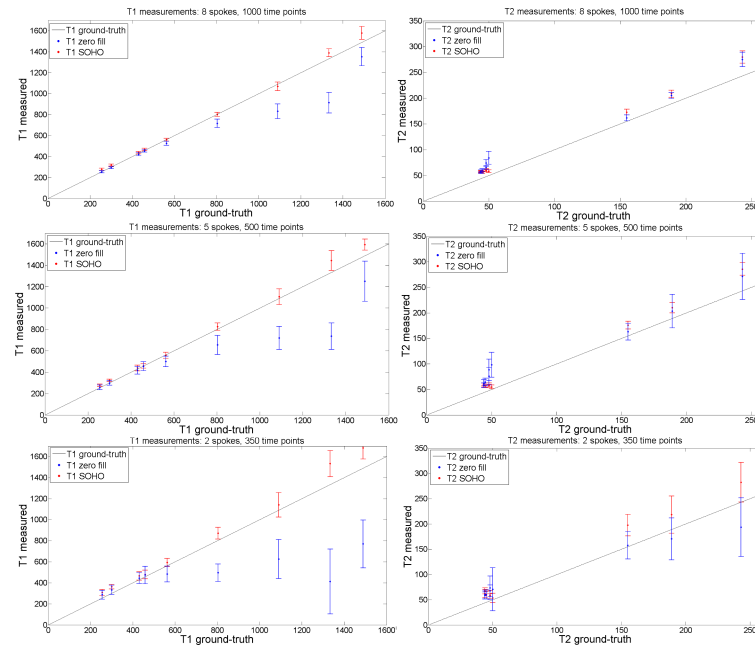


Fig 3. T_1 and T_2 measurement plots (in ms) with zero-filled MRF and the proposed MRF-SOHO reconstructions, using 8 spokes, 1000 time points; 5 spokes, 500 time points; and 2 spokes, 350 time points. An underestimation of T_1 was observed for zero-filled MRF and an overestimation of T_2 was observed for both methods. MRF-SOHO produced more accurate and precise measurements than zero-filled MRF, particularly when less data (time points and radial spokes) was used. Ground truth values were used according to (26).

<https://doi.org/10.1371/journal.pone.0201808.g003>

T_1 , T_2 parametric maps were reconstructed with zero-filled MRF and the proposed MRF-SOHO in the standardized phantom and compared with ground truth values. Plots of the measured T_1 and T_2 values in the phantom $2 \times 2 \text{ mm}^2$ dataset for reconstructions with different amounts of time-point images and with different undersampling factors per time-point image are shown in Fig 3. MRF-SOHO achieved superior accuracy and precision compared to zero-filled MRF for both T_1 (particularly at high T_1 values) and T_2 (particularly at low T_2 values). MRF-SOHO proved robust to higher acceleration factors, whereas zero-filled MRF lost precision and accuracy (particularly underestimation) at higher acceleration factors. Overall, a T_2 overestimation was observed for both methods. A visual inspection (not shown) of the parametric maps with different accelerations revealed MRF-SOHO can be accelerated to 350 time-points using 5 radial spokes while maintaining parametric quality, in line with observations in vivo as shown below.

T_1 and T_2 maps for $2 \times 2 \text{ mm}^2$ dataset using 8, 5 and 2 radial profiles per time-point image and 1000 time-points are shown in Fig 4 for subject 1. Zero-filled MRF achieves good quality T_1 and T_2 maps with 8 radial profiles, but starts failing with higher undersampling factors (5 and 2 radial profiles per time-point image). Conversely, MRF-SOHO achieved superior quality parametric mapping across all undersampling factors, although a slight noise amplification can be observed at higher acceleration factors. Corresponding parametric maps for the same dataset using 1000, 350 and 200 time-point images with 5 radial profiles per time-point are shown in Fig 5. Analogous to the previous figure, the performance of zero-filled MRF breaks down with a reduced number of time-point images. MRF-SOHO proved more robust, however a loss in parametric map quality was observed with 200 time points. These images indicate parametric map quality decreases considerably when less than 350 time-points and less than 5 radial profiles are used, which is in agreement with the phantom data.

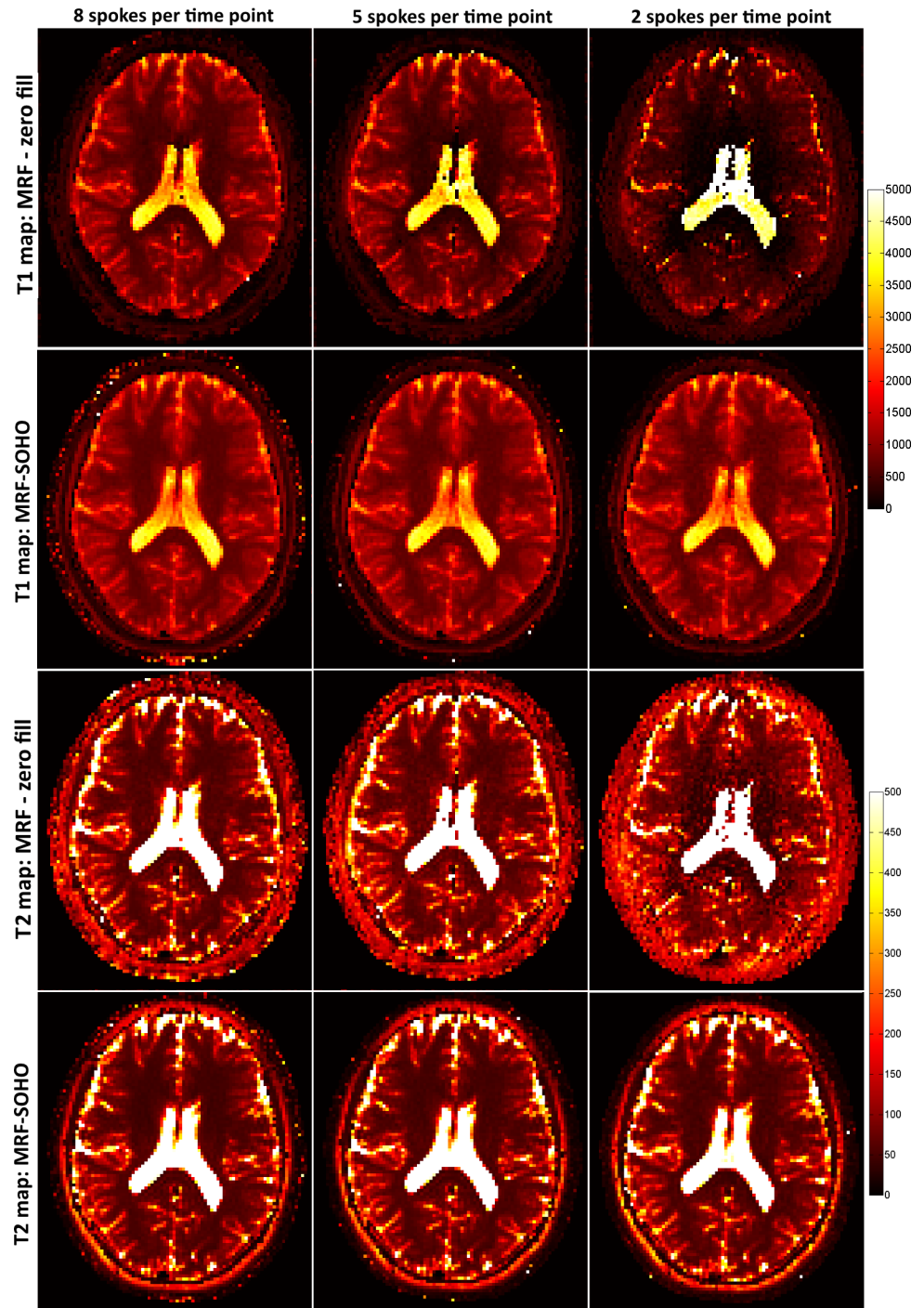


Fig 4. T₁ and T₂ maps (in ms) for zero-filled MRF reconstruction and the proposed MRF-SOHO reconstruction using 1000 time points and different number of radial spokes (8, 5 and 2) for subject 1. The zero-filled MRF reconstruction produces good quality parametric maps with 8 radial spokes, but quickly deteriorates with increased undersampling factor per time-point image. The proposed MRF-SOHO reconstruction produces good quality parametric maps in all cases, however the signal-to-noise ratio is decreased for reduced number of spokes per time point.

<https://doi.org/10.1371/journal.pone.0201808.g004>

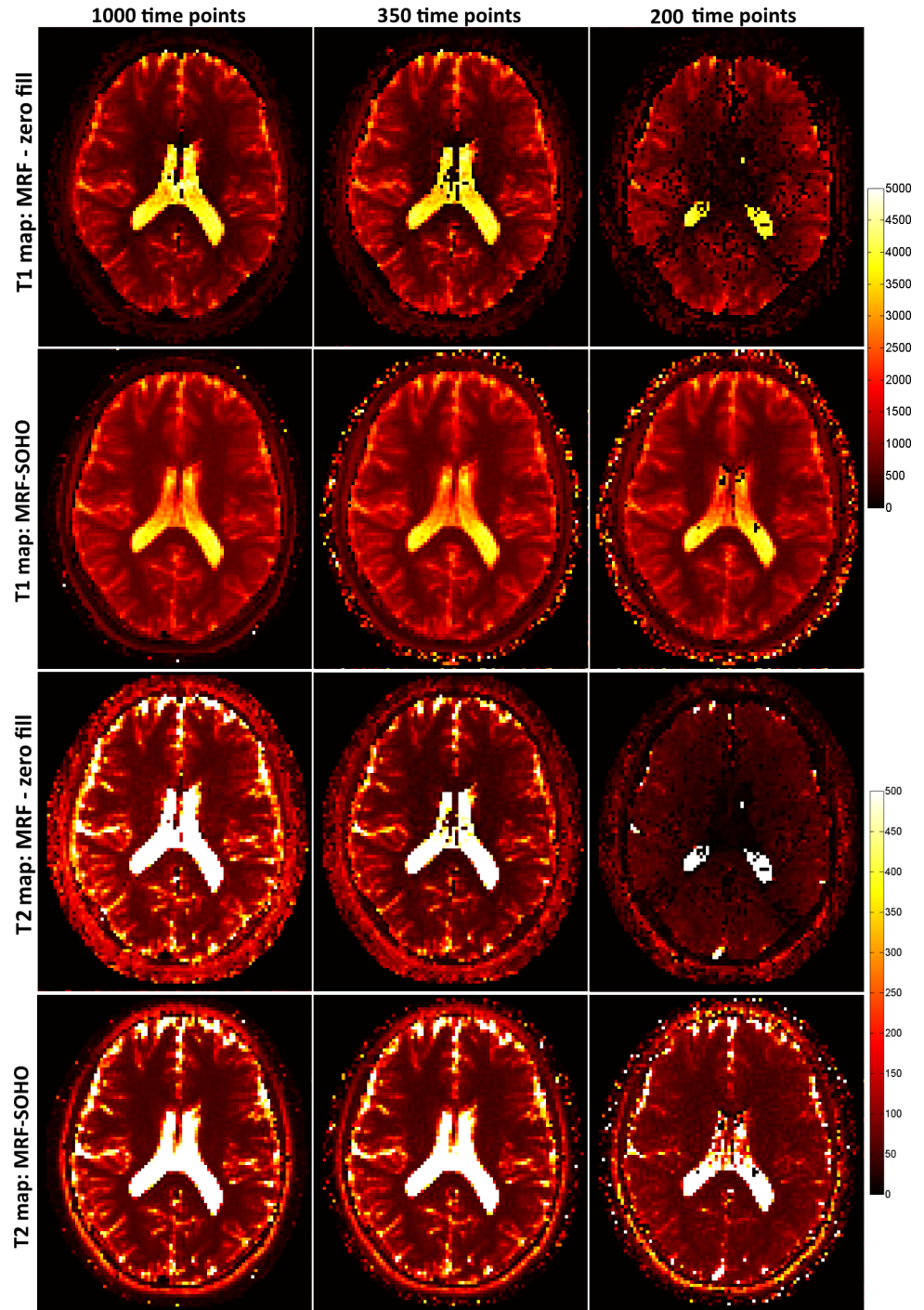


Fig 5. T₁ and T₂ maps (in ms) for zero-filled MRF reconstruction and the proposed MRF-SOHO reconstruction using 5 radial spokes and different number of time points (1000, 350 and 200). The zero-filled MRF reconstruction produces good quality parametric maps with 1000 time points, but starts failing with reduced number of time-point images. The proposed MRF-SOHO reconstruction produces good quality and accurate parametric maps in all cases, however the signal-to-noise ratio is reduced for decreased numbers of time points.

<https://doi.org/10.1371/journal.pone.0201808.g005>

Accelerated MRF-SOHO T₁, T₂ and M₀ parametric maps using 5 radial profiles and 350 time-points are shown in Fig 6 in comparison to the best zero-filled MRF reconstruction (i.e. 8

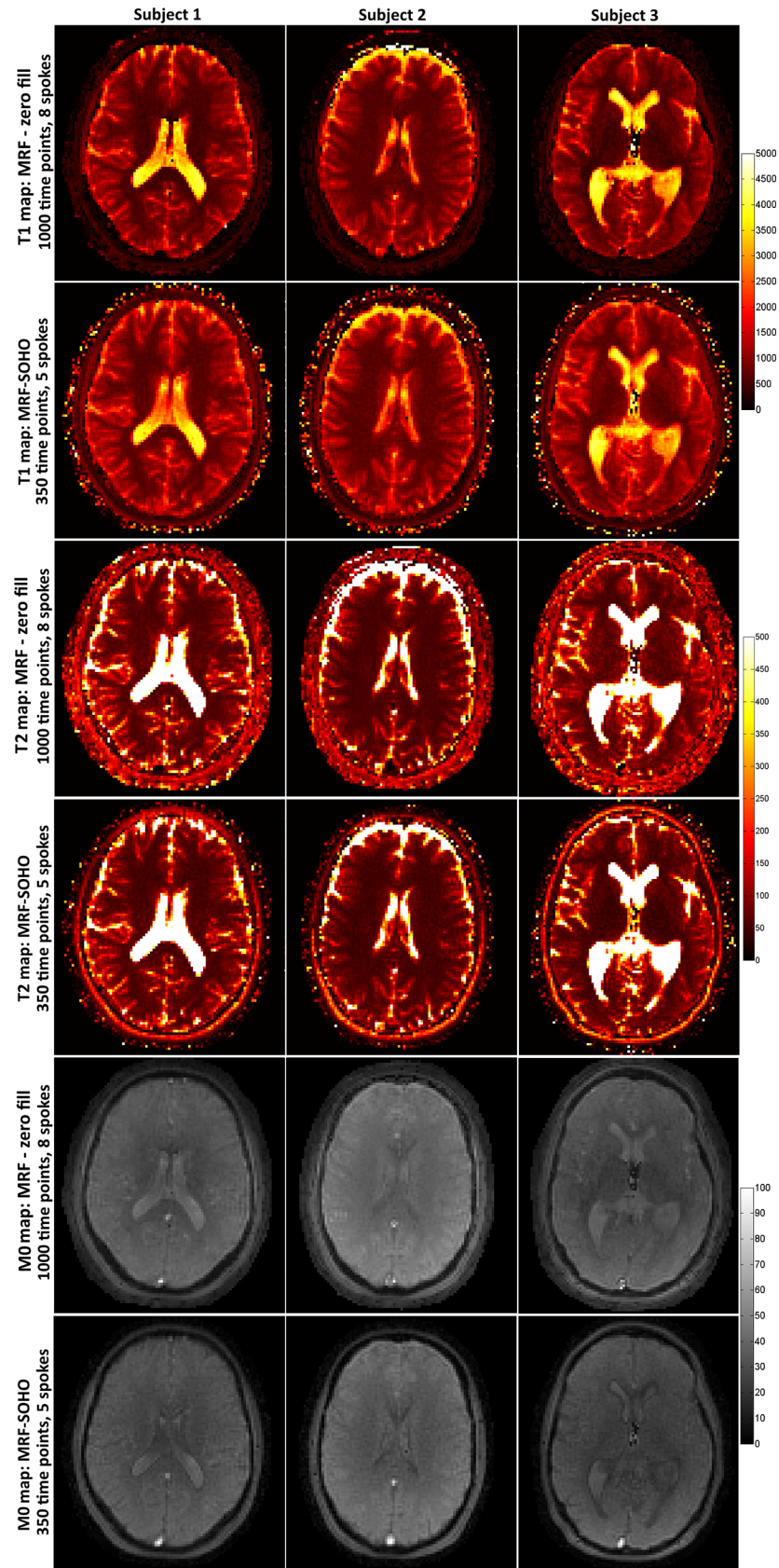


Fig 6. T_1 , T_2 (in ms) and M_0 maps for zero-filled MRF reconstruction (8 spokes, 1000 time-points) and the proposed accelerated MRF-SOHO (5 spokes, 350 time points). The accelerated MRF-SOHO produces similar parametric maps despite a ~4.6x relative acceleration factor to zero-filled MRF.

<https://doi.org/10.1371/journal.pone.0201808.g006>

radial profiles per time-point and 1000 time-point images), for three subjects. MRF-SOHO shows similar quality to zero-filled MRF despite a relative acceleration factor of ~4.6x. T_1 and T_2 values in white matter, grey matter and cerebrospinal fluid (CSF) obtained with zero-filled MRF and the accelerated MRF-SOHO are shown in Table 1, for all subjects. Zero-filled MRF generally underestimated T_1 in white matter and generally overestimated T_2 in grey matter when compared with literature values [30, 31, 32, 33]. This bias was not observed with the proposed MRF-SOHO despite the scan acceleration. Considerable variations in T_1 and T_2 in CSF were observed with both methods in different subjects. Challenges in mapping CSF due to high parametric values, flow and other errors have been reported in other works [34, 35] and require further study.

Plots of measured T_1 and T_2 values in the phantom with $1 \times 1 \text{ mm}^2$ and $0.7 \times 0.7 \text{ mm}^2$ datasets using 8 radial profiles per time-point and 1000 time-point images are shown in Fig 7. The increased undersampling factors per time-point image (~51x for $1 \times 1 \text{ mm}^2$ and ~73x for $0.7 \times 0.7 \text{ mm}^2$ with 8 radial profiles) and reduced signal to noise ratios (SNR) from higher resolutions introduce some errors in the parametric maps using zero-filled MRF, whereas superior accuracy and precision is obtained with the proposed MRF-SOHO.

Parameter maps for the standardized phantom using 8 spokes and 1000 time points reconstructed with zero fill and SOHO are shown in S1 Fig, in correspondence to the plots in Figs 3 and 7. Underestimation bias is observed with zero-filled MRF at higher resolution data (due to higher undersampling factors), whereas accuracy and precision is generally maintained with SOHO. A loss in apparent SNR is observed in both methods, however this degradation is also reduced with SOHO.

T_1 , T_2 and M_0 parametric maps for subject 1 using $2 \times 2 \text{ mm}^2$, $1 \times 1 \text{ mm}^2$ and $0.7 \times 0.7 \text{ mm}^2$ datasets are shown in Fig 8 for zero-filled MRF and the proposed MRF-SOHO using 8 radial profiles and 1000 time points. The proposed MRF-SOHO outperforms zero-filled MRF across all resolution datasets. This is particularly evident at higher resolutions ($0.7 \times 0.7 \text{ mm}^2$), where zero-filled MRF shows considerable degradation due to lower SNR and higher undersampling factor. MRF-SOHO was robust to these conditions, however a reduction in SNR was observed at higher accelerations. The ratio of mean by standard deviation in a ROI in T_1 and T_2 maps was taken as a surrogate for parametric map SNR. Estimated SNR in T_1 for zero-filled reconstruction was approximately 10.7, 4.3 and 4.5, for resolutions $2 \times 2 \text{ mm}^2$, $1 \times 1 \text{ mm}^2$ and $0.7 \times 0.7 \text{ mm}^2$, respectively; corresponding results for SOHO were 26.0, 9.2 and 4.8. Estimated SNR in

Table 1. T_1 and T_2 in healthy subjects.

	T_1 zero-filled	T_1 SOHO	Literature T_1	T_2 zero-filled	T_2 SOHO	Literature T_2
Subject 1: white matter	504±98	691±84	608–756	67±10	52±10	54–81
Subject 1: grey matter	976±152	1146±149	998–1304	118±27	89±17	78–98
Subject 1: CSF	3913±176	3917±220	4103–5400	1941±170	2576±66	1800–2460
Subject 2: white matter	497±53	649±51	608–756	65±11	57±10	54–81
Subject 2: grey matter	959±100	1058±87	998–1304	100±22	90±21	78–98
Subject 2: CSF	3859±148	3821±187	4103–5400	1800±207	2362±336	1800–2460
Subject 3: white matter	627±48	674±54	608–756	54±4	52±6	54–81
Subject 3: grey matter	1064±120	1121±122	998–1304	83±14	80±13	78–98
Subject 3: CSF	2971±407	3057±359	4103–5400	777±115	653±138	1800–2460

<https://doi.org/10.1371/journal.pone.0201808.t001>

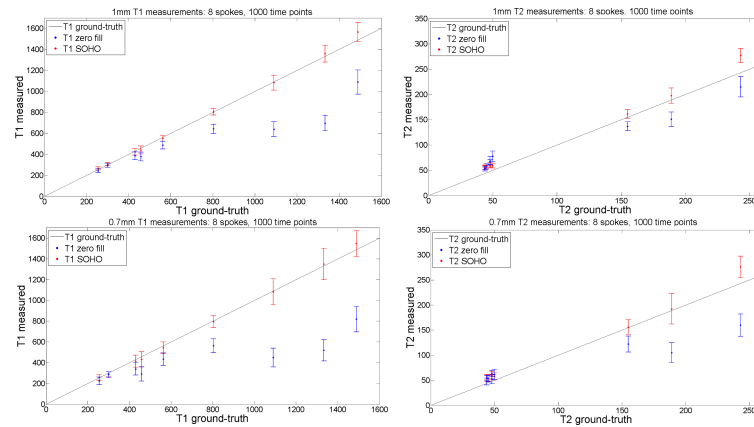


Fig 7. T_1 and T_2 measurement plots (in ms) with zero-filled MRF and the proposed MRF-SOHO reconstructions, using 8 spokes, 1000 time points for 1mm resolution and 0.7 mm² resolution. Analogous to the results in Fig 3, zero-filled MRF underestimated T_1 , particularly at higher resolutions. A slight overestimation of T_2 was observed for the proposed approach, whereas zero-filled MRF considerably underestimated T_2 due to the higher undersampling and reduced SNR.

<https://doi.org/10.1371/journal.pone.0201808.g007>

T_2 for zero-filled reconstruction was approximately 11.6, 5.6 and 5.5, for resolutions 2x2 mm², 1x1 mm² and 0.7x0.7 mm², respectively; corresponding results for SOHO were 18.2, 9.6 and 5.2. Considerable higher SNR was generally observed for SOHO when compared with a zero-filled reconstruction. At higher resolutions, the SNR estimates in zero-filled MRF were affected by the substantial underestimation bias observed in the parametric maps (Fig 8). A similar analysis (not shown here) to the one performed for 2x2mm² resolution dataset suggests the use of 5 profiles, 700 time point images for 1x1 mm² resolution and 8 radial profiles, 700 time-point images for 0.7x0.7 mm² resolution as the most adequate accelerations for MRF-SOHO, respectively. The datasets with 2x2mm², 1x1mm² and 0.7x0.7mm² were acquired in approximately 29, 42 and 52 seconds, respectively. Retrospectively accelerated by SOHO, these scan times were reduced to approximately 6, 18 and 23 seconds.

Discussion

A novel approach for accelerated magnetic resonance fingerprinting acquisition was introduced and validated in a standardized phantom and healthy subject data. The proposed MRF-SOHO combines parallel imaging, soft-weighting and key-hole concepts to reduce aliasing in the highly undersampling time-point images and improves resulting parametric maps. The method shares primarily high frequency information between consecutive time-point images, which is redundant since image contrast evolves slowly when the flip angle is varied smoothly. MRF-SOHO enabled an acceleration factor of ~4.6x relative to zero-filled MRF (considering 8 radial profiles per time-point image and 1000 time points). It was also shown that MRF-SOHO enables sub-millimetric MRF, whereas zero-filled MRF was not robust due to highly increased undersampling artefacts of the time-point images and decreased voxel signal. Additionally, the proposed approach produces high quality time-point images, which may have high diagnostic value when used as a complement to the resulting parametric maps. Alternatively, the unalised time-points could be used for motion estimation, enabling motion correction for MRF [36].

T_1 and T_2 values measured with the proposed approach were generally in agreement with ground-truth phantom measurements and literature values for brain tissues. However, T_2 overestimation was observed in phantom measurements. T_2 overestimation has been observed

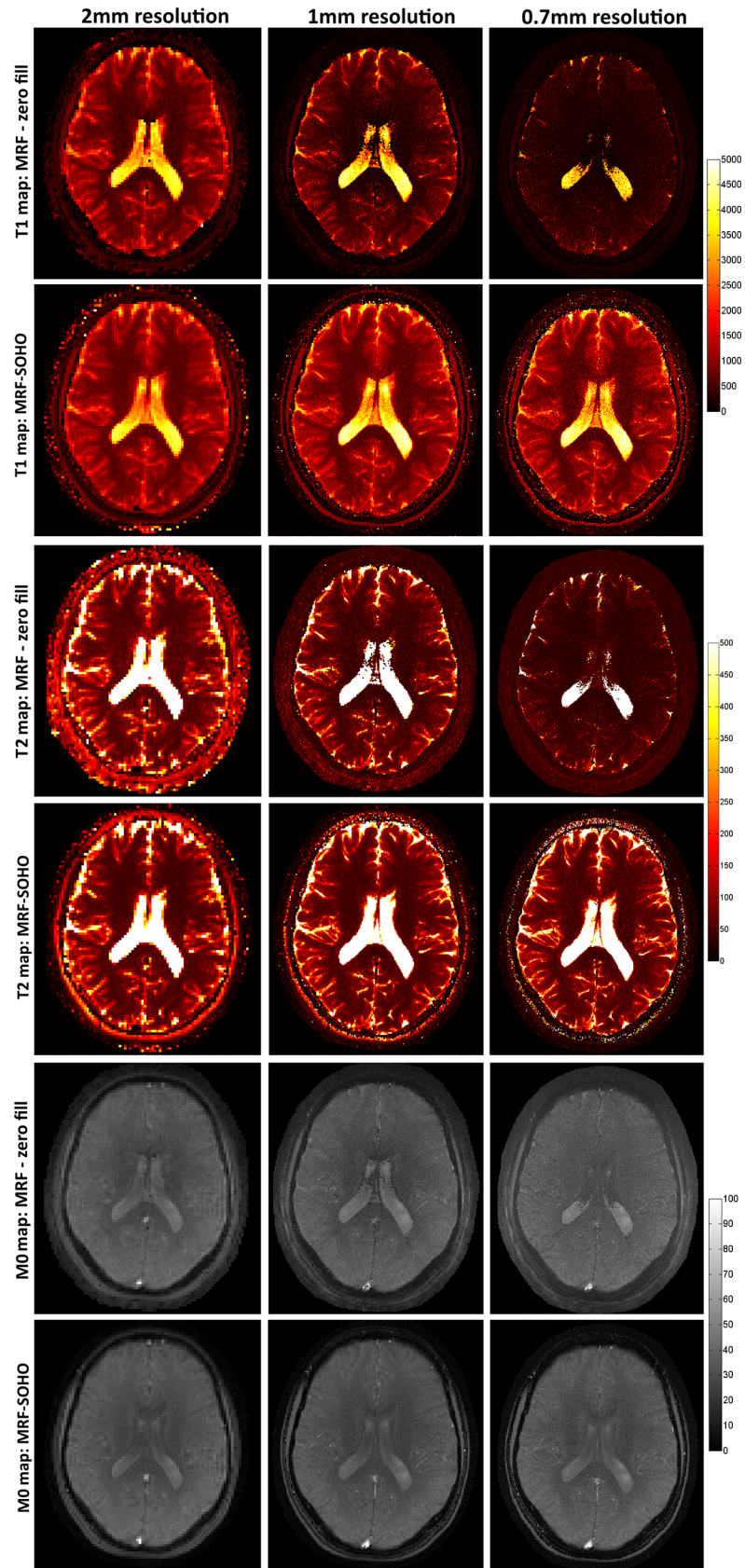


Fig 8. T_1 , T_2 (in ms) and M_0 maps for zero-filled MRF reconstruction and MRF-SOHO using 8 spokes, 1000 time points for 2 mm², 1 mm² and 0.7 mm² resolution in subject 1. Both methods produce comparable parametric maps at 2 mm² resolution, however zero-filled MRF quickly degrades at higher resolutions (and implicitly higher undersampling and noise factors). MRF-SOHO maintained parametric map quality, however a loss in SNR was also observed.

<https://doi.org/10.1371/journal.pone.0201808.g008>

before in [34, 35] and can be addressed with optimised patterns for FA and TR. T_2 bias was also observed for both methods in the CSF, which has also been reported before in [8, 22]. The simulated dictionary B_1 was fixed at 1.0, however B_1 inhomogeneity may introduce errors in the estimated maps, among them the T_2 bias observed for the CSF. Slice profile imperfections in addition to B_1 inhomogeneities have also shown to produce bias in MRF [37]. Flow in the CSF and partial volume effects may also lead to errors in CSF measurements. Additionally, magnetization transfer [38] and coil receiver bias [39] have also been shown to affect T_1 , T_2 and M_0 estimation with MR fingerprinting. Zero-filled MRF presented less accurate phantom results, increased errors at sub-millimetric resolution and/or high acceleration and underestimation of T_1 in the range of white matter and overestimation of T_2 in grey matter. MRF-SOHO produced more accurate parametric maps, despite the relative acceleration factor of 4.6x.

In this work we use a model-based approach for a soft-weighted key-hole reconstruction and determine the data sharing parameters (α , β , μ , τ , N) experimentally, assuming a slow varying flip angle. Incorrect choice of these parameters could affect image contrast of the time-points and potentially introduce a bias in the resulting parameter maps. The optimal data sharing parameters will depend primarily in the sequence parameters (e.g. flip angle pattern) and parameters will have to be tuned for each MRF sequence. However, a data-based approach may provide a more general solution. For instance, singular value decomposition may be used to compress the dictionary and acquired data into a space with reduced number of time points [40]. This analysis is considered as future work and it may reveal further redundancies in the data and therefore enable higher acceleration factors. As MRF will generally operate in highly undersampled regimes, aliasing artefacts may propagate into the parametric maps. Methods like soft-weighting, sliding window, parallel imaging and compressed sensing can reduce these errors. Future work should evaluate the improvements of these different strategies, separately and combined, to investigate how these approaches may be used to accelerate MRF. In this work a golden radial trajectory is used instead of the commonly used spiral trajectory for MRF, to avoid T_2 decay induced blurring and avoid acquisition of repeated k-space positions. However, the proposed reconstruction method is applicable to any trajectory, as long as enough low frequency information is acquired for every time-point and k-space positions within SOHO's shared neighbourhood are minimized to maximize trajectory efficiency.

As in [7], a single inversion pulse is used in the beginning of the acquisition to improve sensitivity to T_1 . The results in [14] demonstrate the improvement of additional magnetization preparation pulses in MRF parametric mapping. Future work should explore additional preparation pulses and combine them with the proposed MRF-SOHO framework. Additionally, improved sensitivity to T_1 and T_2 (and improved SNR) could be achieved with a pseudo b-SSFP [41]. Recent work [35] has also demonstrated the benefit of optimized FA and TR patterns to improve estimation of T_1 and especially T_2 . Future work should also incorporate B_1 into the MRF model, as it has been proposed in [12, 13, 37, 38]. Another main limitation of the proposed approach is the reconstruction time (up to 120 minutes for 0.7x0.7 mm). Currently, the method was implemented in MATLAB, however this can be significantly reduced with GPU implementations [42]. In this study, data was retrospectively undersampled to allow comparisons of different acceleration factors from the same dataset. When evaluating the

number of time-points, a subset of the full set of reconstructed images were retrospectively taken, meaning that the final time-points had access to slightly more high frequency information than in a prospective acquisition, however we consider this difference to be small. The number of golden radial profiles was also retrospectively studied. This means that reconstructions with 5 and 2 profiles do not have a golden angle separation between all angles and may provide suboptimal image quality. A prospective acquisition with 5 radial profiles will potentially have less residual artefacts than the corresponding retrospective acquisition, improving MRF mapping quality and potentially enabling even higher acceleration factors. This work focused on demonstrating the feasibility of MRF-SOHO in healthy subjects. Future work will evaluate this approach in patient studies.

Conclusion

A novel approach for accelerated magnetic resonance fingerprinting (MRF-SOHO) was proposed, achieving comparable parametric maps to zero-filled MRF despite a relative acceleration factor of 4.6x. When using the same acceleration factor, the proposed approach produced superior parametric maps in sub-millimetric MRF when compared to zero-filled MRF.

Supporting information

S1 Video. First 500 time-points for zero-filled gridding (**left**) and MRF-SOHO (**right**) for a 2 mm² resolution dataset.

(AVI)

S2 Video. First 500 time-points for zero-filled gridding (**left**) and MRF-SOHO (**right**) for a 1 mm² resolution dataset.

(AVI)

S3 Video. First 500 time-points for zero-filled gridding (**left**) and MRF-SOHO (**right**) for a 0.7 mm² resolution dataset.

(AVI)

S1 Fig. Parametric maps for the standardized phantom using 1000 time-points and 8 spokes, reconstructed with zero-filled MRF and the proposed SOHO. Underestimation bias is observed with zero-filled MRF at higher resolution data (due to higher undersampling factors), whereas accuracy and precision is generally maintained with SOHO. A loss in apparent SNR is observed in both methods, however this degradation is also reduced with SOHO.

(TIF)

Author Contributions

Conceptualization: Gastao Cruz, Torben Schneider, Tom Bruijnen, Andreia S. Gaspar, René M. Botnar, Claudia Prieto.

Data curation: Gastao Cruz, Torben Schneider.

Funding acquisition: René M. Botnar, Claudia Prieto.

Methodology: Gastao Cruz.

Supervision: René M. Botnar, Claudia Prieto.

Writing – original draft: Gastao Cruz.

Writing – review & editing: Gastao Cruz, Torben Schneider, Tom Bruijnen, Andreia S. Gaspar, René M. Botnar, Claudia Prieto.

References

1. Just M, Thelen M. Tissue characterization with T1, T2, and proton density values: results in 160 patients with brain tumors. *Radiology*. 1988; 169:779–785. <https://doi.org/10.1148/radiology.169.3.3187000> PMID: 3187000
2. Vavasour IM, Whittall KP, Mackay AL, Li DK, Vorobeychik G, Paty DW. A comparison between magnetization transfer ratios and myelin water percentages in normals and multiple sclerosis patients. *Magn Reson Med*. 1998; 40(5):763–768. PMID: 9797161
3. Papadopoulos K, Tozer DJ, Fisniku L, Altmann DR, Davies G, Rashid W, et al. T1-relaxation time changes over five years in relapsing-remitting multiple sclerosis. *Mult Scler*. 2010; 16:427–433. <https://doi.org/10.1177/1352458509359924> PMID: 20086026
4. St Pierre TG, Clark PR, Chua-anusorn W, Fleming AJ, Jeffrey GP, Olynyk JK, et al. Noninvasive measurement and imaging of liver iron concentrations using proton magnetic resonance. *Blood*. 2005; 105:855–861. <https://doi.org/10.1182/blood-2004-01-0177> PMID: 15256427
5. Ghugre NR, Ramanan V, Pop M, Yang Y, Barry J, Qiang B, et al. Quantitative tracking of edema, hemorrhage, and microvascular obstruction in subacute myocardial infarction in a porcine model by MRI. *Magn Reson Med*. 2011; 166:1129–1141.
6. Deoni SC. Quantitative relaxometry of the brain. *Topics in magnetic resonance imaging: TMRI*. 2010 Apr; 21(2):101. <https://doi.org/10.1097/RMR.0b013e31821e56d8> PMID: 21613875
7. Ma D, Gulani V, Seiberlich N, Liu K, Sunshine JL, Duerk JL, et al. Magnetic resonance fingerprinting. *Nature*. 2013; 495:187–192. <https://doi.org/10.1038/nature11971> PMID: 23486058
8. Hennig J, Weigel M, Scheffler K. Calculation of flip angles for echo trains with predefined amplitudes with the extended phase graph (EPG)-algorithm: principles and applications to hyperecho and TRAPS sequences. *Magn Reson Med*. 2004; 51:68–80. <https://doi.org/10.1002/mrm.10658> PMID: 14705047
9. Doneva M, Amthor T, Koken P, Sommer K, Börner P. Matrix completion-based reconstruction for undersampled magnetic resonance fingerprinting data. *Magn Reson Imaging*. <http://doi.org/10.1016/j.mri.2017.02.007>
10. Jiang Y, Ma D, Bhat H, Ye H, Cauley SF, Wald LL, et al. Use of pattern recognition for unaliasing simultaneously acquired slices in simultaneous multislice MR fingerprinting. *Magn Reson Med* 2016. <https://doi.org/10.1002/mrm.26572> PMID: 28019022
11. Rieger B, Zimmer F, Zapp J, Weingärtner S, Schad LR. Magnetic resonance fingerprinting using echo-planar imaging: Joint quantification of T₁ and T2* relaxation times. *Magn Reson Med*. <https://doi.org/10.1002/mrm.26561> PMID: 27981641
12. Buonincontri G, Sawiak SJ. MR fingerprinting with simultaneous B1 estimation. *Magn Reson Med*. 2016; 76:1127–1135. <https://doi.org/10.1002/mrm.26009> PMID: 26509746
13. Cloos MA, Knoll F, Zhao T, Block KT, Bruno M, Wiggins GC, et al. Multiparametric imaging with heterogeneous radiofrequency fields. *Nature communications*. 2016 Aug 16; 7:12445. <https://doi.org/10.1038/ncomms12445> PMID: 27526996
14. Hamilton JI, Jiang Y, Chen Y, Ma D, Lo WC, Griswold M, et al. MR fingerprinting for rapid quantification of myocardial T₁, T₂, and proton spin density. *Magn Reson Med*. <https://doi.org/10.1002/mrm.26216> PMID: 27038043
15. Cauley SF, Setsompop K, Ma D, Jiang Y, Ye H, Adalsteinsson E, et al. Fast group matching for MR fingerprinting reconstruction. *Magn Reson Med*. 2015; 74:523–528. <https://doi.org/10.1002/mrm.25439> PMID: 25168690
16. Pierre EY, Ma D, Chen Y, Badve C, Griswold MA. Multiscale reconstruction for MR fingerprinting. *Magn Reson Med*. 2016; 75: 2481–2492. <https://doi.org/10.1002/mrm.25776> PMID: 26132462
17. Cao X, Liao C, Wang Z, Chen Y, Ye H, He H, et al. Robust sliding-window reconstruction for Accelerating the acquisition of MR fingerprinting. *Magn Reson Med*. <https://doi.org/10.1002/mrm.26521> PMID: 27851871
18. Assländer J, Cloos MA, Knoll F, Sodickson DK, Hennig J, Lattanzi R. Low Rank Alternating Direction Method of Multipliers Reconstruction for MR Fingerprinting. *Magn Reson Med*. <https://doi.org/10.1002/mrm.26639> PMID: 28261851
19. Zhao B, Setsompop K, Ye H, Cauley SF, Wald LL. Maximum likelihood reconstruction for magnetic resonance fingerprinting. *IEEE Trans Med Imaging*. 2016; 35:1812–23. <https://doi.org/10.1109/TMI.2016.2531640> PMID: 26915119

20. Pruessmann KP, Weiger M, Börner P, Boesiger P. Advances in sensitivity encoding with arbitrary k -space trajectories. *Magn Reson Med*. 2001; 46:638–651. PMID: [11590639](#)
21. Johnson KM, Block WF, Reeder SB, Samsonov A. Improved Least Squares MR Image Reconstruction Using Estimates of k -Space Data Consistency. *Magn Reson Med*. 2012; 67(6):1600–1608. <https://doi.org/10.1002/mrm.23144> PMID: [22135155](#)
22. Song HK, Yan L, Smith RX, Xue Y, Rapacchi S, Srinivasan S, et al. Non-Contrast Enhanced 4-D Dynamic MRA with Golden Angle Radial Acquisition and K -space Weighted Image Contrast (KWIC) Reconstruction. *Magn Reson Med*. 2014; 72(6):1541–1551. <https://doi.org/10.1002/mrm.25057> PMID: [24338944](#)
23. Jiang Y, Ma D, Seiberlich N, Gulani V, Griswold MA. MR fingerprinting using fast imaging with steady state precession (FISP) with spiral readout. *Magn Reson Med*. 2015; 74:1621–1631. <https://doi.org/10.1002/mrm.25559> PMID: [25491018](#)
24. Winkelmann S, Schaeffter T, Koehler T, Eggers H, Doessel O. An optimal radial profile order based on the Golden Ratio for time-resolved MRI. *IEEE T Med Imaging*. 2007; 26(1):68–76.
25. Weigel M. Extended phase graphs: Dephasing, RF pulses, and echoes—pure and simple. *J Magn Reson Imaging*. 2015; 41:266–295. <https://doi.org/10.1002/jmri.24619> PMID: [24737382](#)
26. Captur G, Gatehouse P, Kellman P, Heslinga FG, Keenan K, Bruehl R, et al. A T1 and ECV phantom for global T1 mapping quality assurance: The T1 mapping and ECV standardisation in CMR (T1MES) program. *J Cardiovasc Magn Reson*. 2016; 18(1):1.
27. Rasche V, Proksa R, Sinkus R, Bornert P, Eggers H. Resampling of data between arbitrary grids using convolution interpolation. *IEEE T Med Imaging*. 1999; 18(5):385–392.
28. Greengard L, Lee JY. Accelerating the Nonuniform Fast Fourier Transform. *SIAM Review*. 2004; 46(3):443–454.
29. Uecker M, Lai P, Murphy MJ, Virtue P, Elad M, Pauly JM, et al. ESPIRiT—an eigenvalue approach to autocalibrating parallel MRI: Where SENSE meets GRAPPA. *Magn Reson Med*. 2014; 71:990–1001. <https://doi.org/10.1002/mrm.24751> PMID: [23649942](#)
30. Vymazal J, Righini A, Brooks RA, Canesi M, Mariani C, Leonardi M, et al. T1 and T2 in the brain of healthy subjects, patients with Parkinson disease, and patients with multiple system atrophy: relation to iron content. *Radiology*. 1999; 211:489–495. <https://doi.org/10.1148/radiology.211.2.r99ma53489> PMID: [10228533](#)
31. Deoni SC, Peters TM, Rutt BK. High-resolution T1 and T2 mapping of the brain in a clinically acceptable time with DESPOT1 and DESPOT2. *Magn Reson Med*. 2005; 53:237–241. <https://doi.org/10.1002/mrm.20314> PMID: [15690526](#)
32. Whittall KP, Mackay AL, Graeb DA, Nugent RA, Li DK, Paty DW. In vivo measurement of T2 distributions and water contents in normal human brain. *Magn Reson Med*. 1997; 37:34–43. PMID: [8978630](#)
33. Poon CS, Henkelman RM. Practical T2 quantitation for clinical applications. *J Magn Reson Imaging*. 1992; 2:541–553. PMID: [1392247](#)
34. Jiang Y, Ma D, Keenan KE, Stupic KF, Gulani V, Griswold MA. Repeatability of magnetic resonance fingerprinting T_1 and T_2 estimates assessed using the ISMRM/NIST MRI system phantom. *Magn Reson Med*. <https://doi.org/10.1002/mrm.26509> PMID: [27790751](#)
35. Hamilton J, Wright K, Jiang Y, Hernandez-Garcia L, Ma D, Griswold M, et al. Pulse sequence optimization for improved MRF scan efficiency. Proceedings of the 23rd scientific meeting, International Society for Magnetic Resonance in Medicine, Honolulu, p 3386; 2015.
36. Cruz G, Botnar RM, Prieto C. Motion corrected Magnetic Resonance Fingerprinting using Soft-weighted key-Hole (MRF-McSOHO). Proceedings of the 23rd scientific meeting, International Society for Magnetic Resonance in Medicine, Honolulu, p 935. 2017.
37. Ma D, Coppo S, Chen Y, McGivney DF, Jiang Y, Pahwa S, et al. Slice profile and B1 corrections in 2D magnetic resonance fingerprinting. *Magn Reson Med*. <https://doi.org/10.1002/mrm.26580> PMID: [28074530](#)
38. Hilbert T, Kober T, Zhao T, Block TK, Yu Z, Thiran JP, et al. Mitigating the effect of magnetization transfer in magnetic resonance fingerprinting. Proceedings of the 23rd scientific meeting, International Society for Magnetic Resonance in Medicine, Honolulu, p 74. 2017. <https://doi.org/10.1038/nrm.2017.137>
39. Deshmane A, McGivney D, Jiang Y, Ma D, Griswold M. Proton density mapping and receiver bias correction for absolute quantification with MR fingerprinting. Proceedings of the 23rd scientific meeting, International Society for Magnetic Resonance in Medicine, Honolulu, p 1358. 2017.
40. McGivney DF, Pierre E, Ma D, Jiang Y, Saybasili H, Gulani V, et al. SVD compression for magnetic resonance fingerprinting in the time domain. *IEEE Trans Med Imaging* 33(12):2311–22. 2014. <https://doi.org/10.1109/TMI.2014.2337321> PMID: [25029380](#)

41. Assländer J, Glaser SJ, Hennig J. Pseudo Steady-State Free Precession for MR-Fingerprinting. *Magn Reson Med*. <https://doi.org/10.1002/mrm.26202> PMID: 27079826
42. Sorensen TS, Schaeffter T, Noe KO, Hansen MS. Accelerating the nonequispaced fast fourier transform on commodity graphics hardware. *IEEE Trans Med Imaging*. 2008; 27:538–547. <https://doi.org/10.1109/TMI.2007.909834> PMID: 18390350